

Exploiting lattice potentials for sorting chiral particles

David Speer¹, Ralf Eichhorn², and Peter Reimann¹

¹*Universität Bielefeld, Fakultät für Physik, 33615 Bielefeld, Germany*

²*NORDITA, Roslagstullsbacken 23, 10691 Stockholm, Sweden*

Several ways are demonstrated of how periodic potentials can be exploited for sorting molecules or other small objects which only differ by their chirality. With the help of a static bias force, the two chiral partners can be made to move along orthogonal directions. Time-periodic external forces even lead to motion into exactly opposite directions.

PACS numbers: 05.40.-a 05.60.-k, 05.45.-a

Chiral particles are extended objects which are non-superposable with their mirror image. So-called enantiomers, i.e. chemically identical molecular species with opposite chirality play a crucial role in Chemistry, Biology, and Medicine due to the omnipresence of chiral molecules in living organisms but with only one of the two chiral partners actually being present. Accordingly, enantiomers in drugs, pesticides etc. have very different effects on an organism and thus their separation is of great importance. Established methods of separating enantiomers mostly exploit some kind of chiral selector [1], i.e. some materials, structures, or ancillary molecules which themselves exhibit an intrinsic chirality. Their main disadvantage is that essentially every enantiomer species requires a different selector. Therefore, several alternative concepts have recently been put forward. A first promising direction proposes to utilize appropriate microfluidic flows, such as vortices [2] or shear flows [3, 4]. Second, photoinduced separation by means of suitably chosen electromagnetic fields has been theoretically predicted in Ref. [5]. A third approach to exploit a structure without an intrinsic chirality is due to de Gennes [6], predicting qualitatively that, according to Curie's principle [7], small chiral crystals should slide down an inclined plane along directions which slightly differ for the two chiral partners, provided thermal noise is negligible. Here, we further pursue this approach, showing that with the help of periodic potentials the two chiral partners even can be made to move into opposite directions, with remarkable persistence against thermal noise.

Apart from “true” (bio-) molecular enantiomers, we also have in mind chiral nano- and micro-particles, e.g. helically shaped nonmotile bacteria [3] and artificial flagellae [8], carbon nanotubes, chiral colloidal clusters [9], or ferromagnetic nano-propellers [10]. The periodic potentials we are proposing to utilize for sorting those chiral particles may be realized e.g. by means of crystal surfaces [11], optical lattices [12], periodic micro- and nano-structures [13], or magnetic bubble lattices [14].

Most of us are not very accustomed to think in terms of chiral symmetry and symmetry-breaking, especially in combination with the crystal symmetries of a periodic potential. For this reason only, we mainly focus on the simplest possible setup [2], namely the two-dimensional dynamics in a square lattice potential of a “minimal”

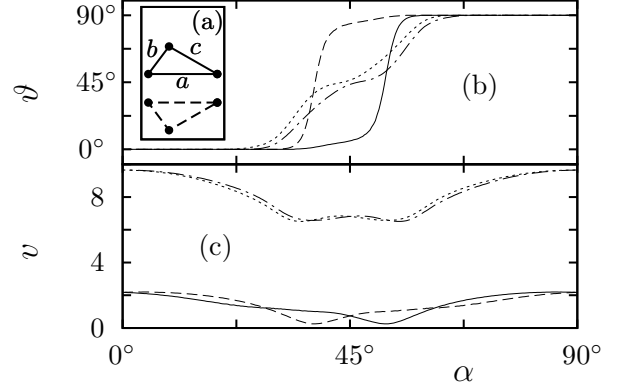


FIG. 1: (a) Solid: Triangle, specified by a, b, c . Dashed: Its chiral partner. (b) and (c): Direction ϑ and modulus v of the net velocity $\vec{v} = \vec{e}_\vartheta v$ versus the direction α of a static bias A in (5) by numerically solving (2)-(6) with parameters as specified below (6). Solid: $kT = 0.08$, $A = 3.6$, $a = 0.4$, $b = 0.23$, $c = 0.34$ (proportional to the solid triangle in (a)). Dashed: Same but for the chiral partner (dashed in (a)). Dashed-dotted and dotted: Same but for $A = 10$.

planar, chiral “molecule”, consisting of three identical, rigidly coupled “atoms” or other small objects with broken mirror symmetry, see Fig. 1a. All basic effects and mechanisms are recovered in three dimensions and also for more general lattices, but are much more cumbersome to visualize and explain. This very general validity of our main results will be exemplified for various other chiral “molecules” in the end. We thus consider the two-dimensional dynamics

$$m_i \ddot{\vec{x}}_i(t) = -\gamma_i \dot{\vec{x}}_i(t) + \vec{F}(\vec{x}_i(t), t) + \vec{f}_i + \vec{\xi}_i(t). \quad (1)$$

Dots indicate time derivatives, $\vec{x}_i = \vec{e}_1 x_{i,1} + \vec{e}_2 x_{i,2}$ are the “atom positions” ($i = 1, 2, \dots, N$) in Cartesian coordinates \vec{e}_ν ($\nu = 1, 2$), m_i their mass, and γ_i their dissipation coefficient, e.g. due to an ambient fluid. In particular, for the triangular particles (Fig. 1a) we have $N = 3$ and i -independent γ_i and m_i . The force field $\vec{F}(\vec{x}, t)$ is partly due to a “lattice potential” (see below) and partly due to an externally applied driving, typically via electrophoresis. Under these conditions, hydrodynamic interactions are screened [15] and therefore safely negligible [2, 3]. The internal constraining

forces, maintaining e.g. the triangular shape in Fig. 1a, are represented by \vec{f}_i , and thermal fluctuations are modelled as usual by unbiased Gaussian white noise $\vec{\xi}_i(t) = \vec{e}_1 \xi_{i,1}(t) + \vec{e}_2 \xi_{i,2}(t)$, satisfying the fluctuation dissipation relation $\langle \xi_{i,\mu}(s) \xi_{j,\nu}(t) \rangle = 2\gamma_i kT \delta_{ij} \delta_{\mu\nu} \delta(s-t)$ with T the ambient temperature and k Boltzmann's constant. The position of the rigid "molecule" is conveniently specified by the so-called center of friction [2] $\vec{X} := \sum_{i=1}^N \gamma_i \vec{x}_i / \sum_{i=1}^N \gamma_i$, and its orientation by the angle ϕ between the \vec{e}_1 axis and the position of "atom 1" relative to the center of friction: $\phi := \angle(\vec{e}_1, \vec{x}_1 - \vec{X})$. Rewriting (1) in terms of \vec{X} and ϕ to get rid of the constraining forces \vec{f}_i is a basic mechanics exercise. Further, for the very small objects we have in mind, inertia effects are negligible [16, 17], yielding [2]

$$\dot{\vec{X}}(t) = \frac{\sum_{i=1}^N \vec{F}(\vec{x}_i(t), t)}{\sum_{i=1}^N \gamma_i} + \vec{\zeta}(t), \quad (2)$$

$$\dot{\phi}(t) = \frac{\vec{e}_3 \cdot \sum_{i=1}^N \vec{y}_i(t) \times \vec{F}(\vec{x}_i(t), t)}{\sum_{i=1}^N \gamma_i y_i^2} + \zeta_\phi(t), \quad (3)$$

$$\vec{x}_i(t) = \vec{X}(t) + \vec{y}_i(t), \quad \vec{y}_i(t) = \mathbf{O}(\phi(t)) \vec{y}_i(0). \quad (4)$$

In (3), vectors are temporally embedded into \mathbb{R}^3 with standard scalar and vector products \cdot and \times . In (4), $\mathbf{O}(\phi)$ is a rotation matrix with elements $O_{11} = O_{22} = \cos \phi$ and $O_{12} = -O_{21} = -\sin \phi$. Thus, $\vec{y}_i(t)$ are the particle positions relative to the center of friction with convention $\phi(0) = 0$ and with t -independent modulus $y_i := |\vec{y}_i(t)|$. Finally, $\vec{\zeta}(t)$ and $\zeta_\phi(t)$ are independent Gaussian white noises with $\langle \zeta_\mu(s) \zeta_\nu(t) \rangle = 2kT \delta_{\mu\nu} \delta(s-t) / \sum \gamma_i$ and $\langle \zeta_\phi(s) \zeta_\phi(t) \rangle = 2kT \delta(s-t) / \sum \gamma_i y_i^2$.

As already said, the force field consists of two parts,

$$\vec{F}(\vec{x}, t) = \vec{e}_\alpha A(t) - \vec{\nabla} U(\vec{x}), \quad (5)$$

namely a spatially homogeneous, externally applied force along the direction $\vec{e}_\alpha := \vec{e}_1 \cos \alpha + \vec{e}_2 \sin \alpha$ and a Gaussian square lattice potential with period L :

$$U(\vec{x}) = u \sum_{m,n=-\infty}^{\infty} \exp\left\{-\frac{(\vec{x} - [m\vec{e}_1 + n\vec{e}_2]L)^2}{2\sigma^2}\right\}. \quad (6)$$

For this potential with $u > 0$ and $u < 0$ as well as for various other potentials we always found similar results. Focusing on $u > 0$ from now on, the natural energy scale is the potential barrier $\Delta U := U(\vec{e}_1 L/2) - U(\vec{0})$ separating adjacent potential wells. We henceforth adopt time, energy, and length units so that $\min_i \gamma_i = 1$, $\Delta U = 1$, $L = 1$, and focus on $\sigma = L/4$ [18].

The quantity of central interest is the net velocity $\vec{v} = \vec{e}_\theta v$, obtained by averaging $\dot{\vec{X}}(t)$ over time. Obviously, rotating the force field (5) by 90° leaves the potential (6) invariant and entails a rotation of \vec{v} by 90° . Hence, it is sufficient to focus on $\alpha \in [0^\circ, 90^\circ]$. Likewise, one readily sees that $A(t) \mapsto -A(t)$ implies $\vec{v} \mapsto -\vec{v}$.

We first consider t -independent A , i.e. the force field (5) derives from a tilted periodic potential. For $A = 0$

symmetry implies $\vec{v} = \vec{0}$. For $A \neq 0$ the salient point is to realize that there exists no symmetry argument why two "molecules" of opposite chirality should travel down the tilted periodic potential with identical velocities \vec{v} . Following de Gennes [6], we thus can invoke Curie's principle to conclude [7, 16] that generically (i.e. up to parameter sets of measure zero) the velocities will indeed be different. In other words, (practically) *any tilted periodic potential can separate chiral partners* via their velocities. The main remaining problem pinpointed by De Gennes is the quantitative efficiency of the effect.

Fig. 1 provides those quantitative details in a typical case. We see that the velocities \vec{v} of the two chiral partners are indeed disappointingly similar, except around $\alpha = 45^\circ$. The explanation is as follows: For small thermal energies kT and small bias A , the particles travel extremely slowly by thermally activated hopping from one local minimum of the tilted periodic potential to the next. For any given orientation α there exists a critical tilt A in (5) at which certain local minima disappear by annihilation (collision) with saddle points, giving rise to "running solutions". For $kT = 0$ (deterministic limit), these solutions travel either parallel to \vec{e}_1 or to \vec{e}_2 , and for small $kT > 0$ still almost so. Roughly speaking, the direction "closer" to that of the static bias $\vec{e}_\alpha A$ is preferred, but due to the broken mirror symmetry, the direction actually switches already at some $\alpha < 45^\circ$ for one chiral partner and symmetrically at $\alpha > 45^\circ$ for the other (solid and dashed in Fig. 1). Since these considerations do not depend on any details of the model we can conclude that *a separation by (almost) 90° is generic for $\alpha = 45^\circ$, small kT , and A close to criticality*. Upon further increasing A , the deterministic running solutions speed up and bifurcate into new ones, "locked" [12, 17] along directions of the form $n\vec{e}_1 + m\vec{e}_2$ with increasingly large integers n and m (dashed-dotted and dotted in Fig. 1) and with $\vec{v} \rightarrow \vec{e}_\alpha A N / \sum \gamma_i$ for $A \rightarrow \infty$. Likewise, for finite kT the deterministically "sharp" bifurcations get washed out (Fig. 1) and $\vec{v} \rightarrow \vec{e}_\alpha A N / \sum \gamma_i$ for $kT \rightarrow \infty$.

Thus focusing on $\alpha = 45^\circ$, the dependence of the velocity \vec{v} on the bias A is shown in Fig. 2 (a,b). For symmetry reasons, *the velocities of the two chiral partners are now equal in modulus and symmetric about $\alpha = 45^\circ$* (see also Fig. 1). Remarkably enough, for some A -values, one triangle moves (practically) parallel to \vec{e}_1 (Fig. 2c) and thus its chiral partner parallel to \vec{e}_2 (not shown in Fig. 2), while for some different A -values it is exactly the other way round (Fig. 2d). In other words, *one and the same triangle may move along orthogonal directions for two different A -values*.

Turning to periodic $A(t)$ in (5), our so far findings quite naturally suggest the following idea: We select $\alpha = 45^\circ$ and two static bias values A_1 and A_2 with velocities $\vec{v}_1 = v_1 \vec{e}_1$ and $\vec{v}_2 = v_2 \vec{e}_2$ (e.g. $A_1 = 4$ and $A_2 = 6$ for the solid lines ($kT = 0.014$) in Fig. 2a,b) and exploit that the signs of v_1 and v_2 can be arbitrarily chosen by adjusting the signs of A_1 and A_2 (recall that $A \mapsto -A$ implies $\vec{v} \mapsto -\vec{v}$). If we now construct a time-periodic

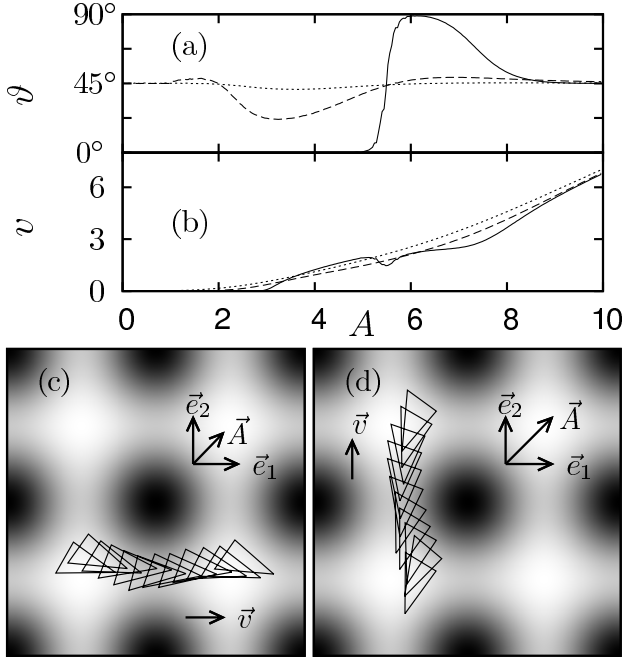


FIG. 2: (a) and (b): Direction ϑ and modulus v of the net velocity $\vec{v} = \vec{e}_\vartheta v$ for the solid triangle from Fig. 1a versus static bias A with fixed direction $\alpha = 45^\circ$. Shown are numerical solutions of (2)-(6) for $kT = 0.014$ (solid), $kT = 0.16$ (dashed), and $kT = 0.32$ (dotted). Other parameters as in Fig. 1. (c) and (d): Illustration of the triangle's motion for $A = 4$ (c) and $A = 6$ (d) at $kT = 0.014$. The static bias is indicated by $\vec{A} := \vec{e}_\alpha A$ and the periodic potential (6) as "shaded background". The triangle motion is shown for a time-span of about 14.5 time-units in (c) and about 8.5 in (d), and then continues periodically up to noise effects (not shown).

$A(t)$ which takes the value A_1 during a fraction $p \in [0, 1]$ of its total period τ and the value A_2 during the rest of the period, the resulting time averaged velocity will be $\vec{v} = p\vec{v}_1 + (1-p)\vec{v}_2$, provided τ is so large that transient effects after each jump of $A(t)$ are negligible. Therefore, the molecule can be steered into *any* direction on the two-dimensional plane by varying p and adapting the signs of $A_{1,2}$. In particular, we will encounter a situation where \vec{v} is orthogonal to the force direction \vec{e}_α . E.g. from the solid lines in Fig. 2 we can read off that the triangle will move with such a velocity $\vec{v} \perp \vec{e}_\alpha$ if we choose $A_1 = -4$, $A_2 = 6$, and $p \approx 2/3$ to account for the difference in modulus of the corresponding velocities $\vec{v}_1 \approx -1.2\vec{e}_1$ and $\vec{v}_2 \approx 2.4\vec{e}_2$. The net velocity \vec{v} of the chiral partner follows from the above mentioned symmetry about $\alpha = 45^\circ$: This symmetry applies to both \vec{v}_1 and \vec{v}_2 separately, and hence also to $\vec{v} = p\vec{v}_1 + (1-p)\vec{v}_2$. Altogether, *the two chiral partners can thus be forced to move into exactly opposite directions*. Deviations due to the so far neglected transient effects after each jump of $A(t)$ are – at least for not too small τ -values – small and thus can be compensated by adjusting p and/or $A_{1,2}$.

Fig. 3 shows that these ideas indeed work out in prac-

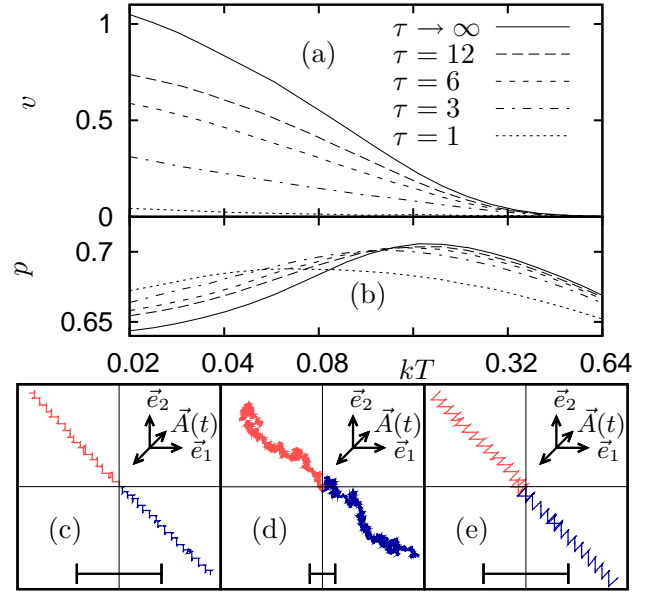


FIG. 3: (a): Absolute velocity v versus thermal energy kT (logarithmic scale) for the same system as in Fig. 1 but with a τ -periodic driving $\vec{e}_\alpha A(t)$ with $\alpha = 45^\circ$ and $A(t)$ taking the value $A_1 = -4$ during a fraction p of the period τ and the value $A_2 = 6$ during the rest of the period. (b): The corresponding p -values, adjusted as described in the main text so that the two chiral partners move into exactly opposite directions. (c) Typical single-particle trajectories $\vec{X}(t)$ for the two chiral partners (light red and dark blue) with $t \in [0, 100]$, $\vec{X}(0) = \vec{0}$, $kT = 0.02$, $p = 0.66$, and $\tau = 6$. Other parameters as in (a). The bar indicates 50 lattice periods and the double arrow the periodic driving [18]. (d) Same but for a much larger thermal energy $kT = 0.32$ and $t \in [0, 6000]$, $p = 0.69$. (e) Same as in (c) but for a very different triangle with $a = 2.5$, $b = 2.2$, $c = 1.1$ (cf. Fig. 1), and a driving with $A_1 = -7$, $A_2 = 14$, $p = 0.8$ [18].

tice, and in fact down to surprisingly small time-periods τ and up to remarkably large thermal energies kT . Note that while the velocities in Fig. 3a are long-time averages, Figs. 3c-e exemplify single-particle trajectories of moderate duration. Hence the thermal noise still leads to quite notable random fluctuations of each trajectory $\vec{X}(t)$ around the average behavior, especially in Fig. 3d. Only in Figs. 3c,e we still can see the expected "steps" of $\vec{X}(t)$ at jumps of $A(t)$.

Our above recipe for tailoring transport directions can be readily extended to arbitrary velocities \vec{v}_1 and \vec{v}_2 , provided they are not parallel to each other: Then, as before, $\vec{v} = p\vec{v}_1 + (1-p)\vec{v}_2$ can be made to point along any direction by properly choosing p and the signs of $A_{1,2}$. Intuitively and in view of Fig. 2, it is quite clear that generically one will always be able to find two bias values A_1 and A_2 with non-parallel velocities \vec{v}_1 and \vec{v}_2 . We thus can conclude that *chiral partners can (practically) always be made to move into opposite directions by means of a suitably tailored periodic driving force*. Fig. 3e exemplifies this generalized theoretical scheme for comparatively

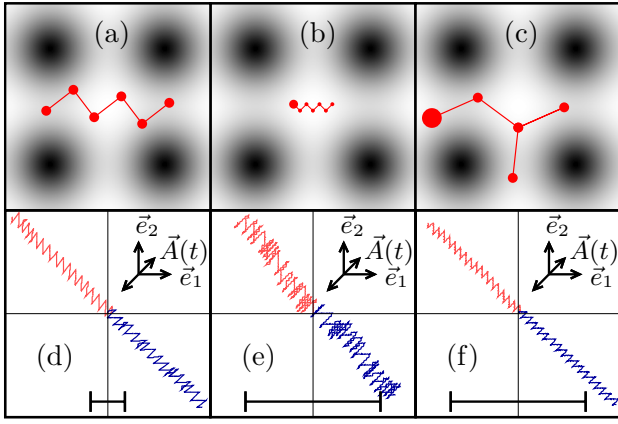


FIG. 4: (a)-(c): Further examples of chiral “molecules”. Dots indicate the constituting “atoms”, lines their rigid coupling, and the “shaded background” the periodic potential (6). Adopting units as specified below (6), $\gamma_i = 1$ for all “atoms” except for the larger dots in b and c, representing $\gamma_i = 3$. (d) Typical single-particle trajectories $\vec{X}(t)$ for the molecule from (a) and its chiral partner (light red and dark blue), obtained by numerically simulating (2)-(6) with $t \in [0, 100]$, $\vec{X}(0) = \vec{0}$, and $kT = 0.02$. Parameters of the periodic driving (see main text): $\alpha = 45^\circ$, $A_1 = 7.8$, $A_2 = -11.7$, $\tau = 6$, $p = 0.71$. The bar indicates 50 lattice periods and the double arrow the periodic driving. (e): Same but for the “molecule” from (b) and $A_1 = 7$, $A_2 = -10.5$, $p = 0.78$ [18]. (f): Same but for the “molecule” from (c) and $A_1 = 3$, $A_2 = -6$, $p = 0.85$ [18].

“large” triangular particles and Fig. 4 for a representative selection of more general chiral “molecules”. Generalizations involving more than two “static velocities” \vec{v}_i and the concomitant optimization problems point into interesting directions for future research.

In conclusion, periodic potentials can act as very effective and versatile selectors for sorting small objects which only differ by their chirality. Static bias forces make the two chiral partners move into directions which differ by up to 90° (Figs. 1,2). Appropriately chosen time-periodic forces even lead to motion into exactly opposite directions (Figs. 3,4). A major advantage compared to many other separation concepts [1] is that one and the same periodic potential may act as an efficient selector for quite different chiral particle species by suitably adapting the time-periodic driving force. Furthermore, the separation mechanisms are remarkably robust against thermal noise. The basic symmetry breaking conditions at the origin of all these effects are generically satisfied for much more general systems than in (1)-(6), including three spatial dimensions, finite inertia effects, other chiral objects and crystal potentials. An experimental proof of principle for chiral micro-particles [8–10] moving in a periodically structured microfluidic device [13] is presently under construction in the Anselmetti lab at Bielefeld University.

This work was supported by Deutsche Forschungsgemeinschaft under SFB 613 and RE1344/5-1

-
- [1] S. Ahuja (Editor), Chiral Separations: Applications and Technology, Amer. Chemical Soc. (1997); Chiral Separation Methods for Pharmaceutical and Biotechnological Products, Wiley (2010)
 - [2] M. Kostur, M. Schindler, P. Talkner, and P. Hänggi, Phys. Rev. Lett. **96**, 014502 (2006)
 - [3] Marcos, H. C. Fu, T. R. Powers, and R. Stocker, Phys. Rev. Lett. **102**, 158103 (2009)
 - [4] N. Watari and R. G. Larson, Phys. Rev. Lett. **102**, 246001 (2009)
 - [5] B. Spivak and A. V. Andreev, Phys. Rev. Lett. **102**, 063004 (2009)
 - [6] P. G. de Gennes, Europhys. Lett. **46**, 827 (1999)
 - [7] P. Curie, J. Phys. (Paris) 3. Série (théorique et appliqué) t. III (1894) 393.
 - [8] L. Zhang et al, Appl. Phys. Lett. **94**, 064107 (2009)
 - [9] D. Zerrouki et al, Nature **455**, 380 (2008)
 - [10] A. Gosh and P. Fischer, Nano Lett. **9**, 2243 (2009)
 - [11] S. Miret-Artés and E. Pollak, J. Phys. Condens. Matter **17**, S4133 (2005).
 - [12] P. T. Korda, M. B. Taylor, and D. G. Grier, Phys. Rev. Lett. **89**, 128301 (2002); M. P. MacDonald, G. C. Spalding, and K. Dholakia, Nature **426**, 421 (2003); K. Xiao and D. G. Grier, Phys. Rev. Lett. **104**, 028302 (2010)
 - [13] S. W. Turner et al. J. Vac. Sci. Technology B **16**, 3835 (1998) M. Carbodi et al., Electrophoresis **23**, 3496 (2002) N. Kaji et al. Anal. Chem. **76**, 15 (2004); J. Fu et al, Nature Nanotech. **2**, 121 (2007)
 - [14] P. Tierno, T. H. Johansen, and T. M. Fischer, Phys. Rev. Lett. **99**, 038303 (2007); P. Tierno, A. Soba, T. H. Johansen, and F. Sagués, Appl. Phys. Lett. **93**, 214102 (2008).
 - [15] D. Long, J.-L. Viovy, and A. Ajdari, Phys. Rev. Lett. **76**, 3858 (1996).
 - [16] P. Reimann, Phys. Rep. **361**, 57 (2002).
 - [17] C. Reichhardt and F. Nori, Phys. Rev. Lett. **82**, 414 (1999); M. Pelton, K. Ladavac, and D. G. Grier, Phys. Rev. E **70**, 031108 (2004); A. Gopinathan and D. G. Grier, Phys. Rev. Lett. **92**, 130602 (2004); A. M. Lacasta, J. M. Sancho, A. H. Romero, and K. Lindenberg, Phys. Rev. Lett. **94**, 160601 (2005); J. P. Gleeson, J. M. Sancho, A. M. Lacasta, and K. Lindenberg, Phys. Rev. E **73**, 041102 (2006); M. Balvin et al. Phys. Rev. Lett. **103**, 078301 (2009)
 - [18] For example, $L \approx 1 \mu\text{m}$, $T \approx 293 \text{ K}$, and $\min_i \gamma_i \approx$ Stokes friction in water of a sphere with radius $r \approx L/10$ yields $v \approx 25 \mu\text{m/s}$ and $\tau \approx 0.1 \text{ s}$ in Fig. 3c, e and Fig. 4e, f.